Supplementary Information

An Alloy Small Molecule Acceptor for Green Printing Organic Solar Cells Overcoming the Scaling Lag of Efficiency

Ji Wan[1], Yao Wu[1], Rui Sun[1], Jiawei Qiao[2], Xiaotao Hao[2], Jie Min[1*]

[1]The Institute for Advanced Studies, Wuhan University, Wuhan 430072, China

E-mail: min.jie@whu.edu.cn

[2]School of Physics, State Key Laboratory of Crystal Materials, Shandong University, Jinan 250100, P.R. China

1. Experimental Section

1.1. Materials

Materials: PM1 and YC12-CHO were purchased from Solarmer Materials Inc. L8-BO was purchased from eFlex PV. The BTP-F3Cl acceptors were synthesized via Knoevenagal reaction. The detailed procedures are described in the following. Other reagents and solvents used were purchased from commercial sources and used as received.
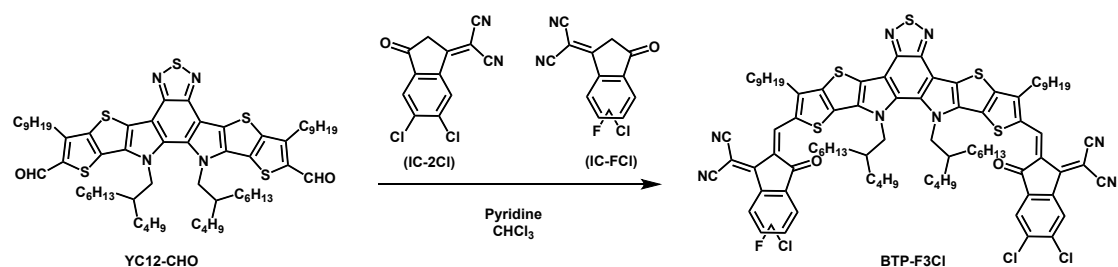
Scheme 1: Synthesis route of small molecule acceptor **BTP-F3Cl**.

YC12-CHO (300 mg, 0.277 mmol), IC-2Cl (87 mg, 0.332 mmol), IC-FCl (82 mg, 0.332 mmol) and chloroform (30 mL) were added into a round bottom flask under nitrogen, followed by pyridine (0.5 mL) dropwise. The mixture was refluxed overnight. After cooling to room temperature, the mixture was poured into methanol and filtered. The residue was purified with column chromatography on silica gel using chloroform/petroleum (2:1) as the eluent to give a dark blue solid **BTP-F3Cl** (136 mg, 31.5% yield). ^{1}H NMR spectra for **BTP-F3Cl**: ^{1}HNMR (600 M, CDCl$_3$) δ. 1H NMR (600 MHz, CDCl$_3$) δ 9.15 (s, 2H), 8.77 (d, J = 4.4 Hz, 1H), 8.48 (d, J = 8.9 Hz, 1H), 7.94 (d, J = 8.4 Hz, 2H), 4.78 (t, J = 6.8 Hz, 4H), 3.22 (q, J = 6.6 Hz, 4H), 2.17 – 2.09 (m, 2H), 1.87 (p, J = 8.0 Hz, 4H), 1.51 (q, J = 8.4 Hz, 4H), 1.37 (d, J = 7.4 Hz, 4H), 1.27 (dd, J = 20.5, 6.4 Hz, 20H), 1.22 – 0.90 (m, 28H), 0.87 (t, J = 7.0 Hz, 9H), 0.73-0.63 (m, 13H).

^{13}CNMR spectra for **BTP-F3Cl**: ^{13}C NMR (151 MHz, CDCl$_3$) δ 186.19, 186.03, 162.58, 158.71, 154.10, 153.97, 147.50, 145.30, 145.25, 139.86, 139.53, 139.16,

138.75, 137.71, 136.34, 136.20, 136.07, 135.76, 135.58, 135.51, 134.27, 133.61, 133.44, 131.18, 131.03, 126.90, 125.78, 124.95, 119.93, 115.07, 115.01, 114.59, 113.64, 113.59, 113.51, 55.73, 39.21, 31.87, 31.63, 31.60, 31.24, 30.49, 30.39, 29.84, 29.72, 29.46, 29.31, 28.04, 27.88, 25.47, 25.28, 22.84, 22.79, 22.68, 22.51, 22.49, 14.12, 14.06, 14.04, 13.79, 13.76. MALDI-TOF MS (m/z): 1556.3393

1.2. Relevant morphological and physical characterizations

Contact angle measurements and surface energy calculation: The contact angles of two polymer acceptors (L8-BO and BTP-F3Cl) and polymer donor PM1 were measured using a Contact Angle Analyzer. The contact angles of two different solvents (water and ethylene glycol (EG)) on the neat films were used to calculate the surface tension of each film.

J-V and EQE measurements: The *J-V* characteristics of the OSCs were measured under a 100 mW cm^{-2} AM 1.5G solar simulator (SSF5-3A, Enlitech). The external quantum efficiency (EQE) spectra were recorded using a solar cell spectral response measurement system QE-R3011 (Enli Technology Co., Ltd.), which had been calibrated by a monocrystalline silicon solar cell.

Ultraviolet-visible-near-IR spectroscopy measurements: *UV-vis-NIR* absorption was measured using a PerkinElmer Lambda 1050 Spectrometer.

Cyclic voltammetry (CV) measurements: Electrochemical measurements were carried out at room temperature in an acetonitrile solution of 0.1 mol L^{-1} Bu$_4$NPF$_6$ using ferrocene (-4.8 eV) as a standard reference, with a computer-controlled CHI660C electrochemical workstation. All cyclic voltammetry (CV) curves were measured by films cast from CHCl$_3$ solution on the glassy carbon electrode with Pt wire as the counter electrode and Ag/AgCl as a reference electrode.

Photoluminescence quantum yield (PLQY) measurements: The PLQY of glasses embedded with L8-BO, L8-BO:BTP-F3Cl (1:0.2, wt%) and BTP-F3Cl films were measured using a *UV-NIR* quantum yield spectrometer (C13534, Quantaurus-QY Plus,

Hamamatsu, Japan).

Space charge limited current (SCLC) measurements: Single carrier devices were fabricated and the dark current-voltage characteristics were measured and analyzed in the space charge limited (SCL) regime following the references. The single carrier devices were fabricated (the structure Glass/ITO/PEDOT:PSS/Active layer/MoO$_3$ (10nm)/Ag (100 nm) for hole-only devices and the structure was Glass/ITO/ZnO/Active layer/PNDIT-F3N/Ag for the electron only devices) and the dark current-voltage characteristics measured and analyzed in the space charge limited (SCL) regime. The *J-V* characteristics of both hole-only and electron-only diodes can be excellently fit obeyed the Mott-Gurney law, which can be expressed as the following equation:

$$J = \frac{9}{8}\varepsilon_0\varepsilon_r\mu\frac{V^2}{L^3}exp(\frac{0.89\beta}{\sqrt{L}}\sqrt{V})$$

(1)

Where *J* is current density, μ is the carrier mobility, $\varepsilon_0\varepsilon_r$ is the dielectric permittivity, *L* is the thickness of the active layer of corresponding devices and the β is the field activation factor. $V = V_{appl} - V_{bi}$, V_{appl} is the applied potential, and V_{bi} is the built-in potential that results from the difference in the work function of the anode and the cathode (in this device structure, $V_{bi} = 0.2$ V).

Experimental details of transient absorption spectroscopy: Femtosecond transient absorption spectroscopy measurements were performed on an Ultrafast Helios pump-probe system in collaboration with a regenerative amplified laser system from Coherent. An 800 nm pulse with a repetition rate of 1kHz, a length of 100 fs, and an energy of 7 mJ/pluse, was generated by an Ti: sapphire amplifier (Astrella, Coherent). Then the 800 nm pulse was separated into two parts by a beam splitter. One part was coupled into an optical parametric amplifier (TOPAS, Coherent) to generate the pump pulses at 800 nm. The other part was focused onto a YAG plate to generate white light supercontinuum as the probe beams with spectra covering 750-1600 nm. The time delay between the pump and probe was controlled by a motorized optical delay line with a

maximum delay time of 8 ns. The sample films were spin-coated onto the 1 mm-thick quartz plates and encapsulated by epoxy resin in a nitrogen-filled glove box to resist water and oxygen in the air. The pump pulse is chopped by a mechanical chopper at 500 Hz and then focused on the mounted sample with probe beams. The probe beam was collimated and focused into a fiber-coupled multichannel spectrometer with a CCD sensor. The energy of the pump pulse was measured and calibrated by a power meter (PM400, Thorlabs).

Photo-induced charge carrier extraction by linearly increasing the voltage (photo-CELIV) measurements: In photo-CELIV measurements, the devices were illuminated with a 405 nm laser diode. Current transients were recorded across the internal 50 Ω resistor of our oscilloscope. Here, a fast electrical switch was used to isolate the device to prevent carrier extraction or sweep out. After the variable delay time, the switch connected the device to a function generator. It applied a linear extraction ramp, which was 40 μs long and 2.0 V high. Moreover, it started with an offset matching the V_{OC} of the device for each delay time. To determine the mobility in the devices, photo-CELIV curves were measured using different experimental conditions, differing in delay time and applied voltage.

Grazing incidence X-ray scattering (GIWAXS) measurement: The grazing incidence X-ray scattering (GIWAXS) measurement was carried out with a Xeuss 2.0 SAXS/WAXS laboratory beamline using a Cu X-ray source (8.05 keV, 1.54 Å) and a Pilatus3R 300K detector. The incident angle was 0.13°. The samples for GIWAXS measurements were fabricated on silicon substrates.

Morphological characterizations: Atomic force microscopy (AFM) measurements were performed by using a Nano Wizard 4 atomic force microscopy (JPK Inc. Germany) in Qi mode to observe the film's surface morphologies. All tests were carried out on Bruker MultiMode 8 AFM with the NanoScope V controller. Tapping mode tests parallel to the direction of stretching using Tap300Al-G silicon probes (tip radius: <10 nm; spring constant: 40 N/m; frequency: 300 kHz). Nanomechanical mapping measurements vertical to the sample stretching direction was operated at force-volume

mode, using an E scanner and Multi75AL-G silicon probes. The trigger threshold of the cantilever deflection was set to 3.0 nm.

The detailed calculation processes of exciton diffusion length: Exciton diffusion length can be determined by pump fluence depending on TAS measurement. The 2D images and corresponding decay profiles of excitons in L8-BO, L8-BO:BTP-F3Cl and BTP-F3Cl phases are shown in **Figure S9**. The exciton decay dynamics characterized by TA spectroscopy can be described approximately as:

$$N(t) = \frac{N(0)e^{(-\kappa t)}}{1 + \frac{\alpha}{2\kappa}N(0)[1 - e^{(-\kappa t)}]}$$

(2)

where κ is the bimolecular decay rate constant and α is the singlet−singlet bimolecular exciton annihilation rate, which can be applied to determine the 3D exciton diffusion coefficient:

$$D = \frac{\alpha}{8\pi R}$$

in which D is the diffusion coefficient, R is the annihilation radius of singlet exciton, here we used the generally assumed value of 1 nm.[1] The exciton diffusion length can be calculated by the following equation [2]:

$$L_D = (D\tau)^{1/2}$$

The lifetime τ of L8-BO, BTP-F3Cl and L8-BO:BTP-F3Cl GSB kinetics is 32.19, 4.07 and 9.89 ps, respectively. Therefore, the corresponding κ values are 31.07×10^{-3}, 245.70×10^{-3} and 101.11×10^{-3} ps^{-1}, as shown in **Table S4**. The values of D are 15.96, 20.44 and 115.74 nm^2 ps^{-1}, respectively. Note that the difference in exciton diffusion length is mainly due to the various exciton diffusion coefficients, which correspond to the diffusion rate.[3]

Transient photocurrent (TPC) measurements: Relevant solar cells were excited with a 405 nm laser diode. The transient photocurrent response of the devices at a short circuit condition to a 200 μs square pulse from the LED with no background illumination. The current traces were recorded on a Tektronix DPO3034 digital

oscilloscope by measuring the voltage drop over a 5-ohm sensor resistor in series with the solar cell. DC voltage was applied to the solar cell with an MRF544 bipolar junction transistor in a common collector amplifier configuration.

Transient photovoltage (TPV) measurements: In the TPV measurements, a 405 nm laser diode was used to keep the organic solar cells in the V_{OC} conditions. Measuring the light intensity with a highly linear photodiode and driving the laser intensity with a waveform generator (Agilent 33500B) at one sun. Moreover, a small perturbation was induced with a second 405 nm laser diode. The intensity of the short laser pulse was adjusted to keep the voltage perturbation below 10 mV. After the pulse, the voltage decays back to its steady state value in a single exponential decay.

Electroluminescence Measurement: The EL signature was collected with a monochromator and detected with an InGaAs detector. The data collection range is 700-1300 nm.

FTPS-EQE spectra measurements: The FTPS measurements were recorded using a Bruker Vertex 70 Fourier-transform infrared (FTIR) spectrometer, equipped with a quartz tungsten halogen lamp, a quartz beam-splitter, and an external detector option. A low noise current amplifier (Femto DLPCA-200) was used to amplify the photocurrent produced on the illumination of the photovoltaic devices with light modulated by the FTIR. The output voltage of the current amplifier was fed back into the external detector port of the FTIR. The photocurrent spectrum was collected by FTIR's software.

EQE-EL Measurement: Electroluminescence (EL) quantum efficiency (EQE_{EL}) measurements were performed by applying external voltage sources through the devices from 1 V to 4 V. A Keithley 2400 Source Meter was used for supplying voltages and recording injected current, and a Keithley 485 picoammeter was used for measuring the emitted light intensity.

Device Fabrication and Testing: Solar cell devices fabrication: The solar cell devices were fabricated with a structure of Glass/ITO/PEDOT:PSS(4083)/Active layer/PNDIT-F3N/Ag. Pre-patterned ITO-coated glass substrates were washed with methylbenzene, deionized water, acetone, and isopropyl alcohol in an ultrasonic bath for 15 minutes

each. After blow-drying with high-purity nitrogen, all ITO substrates are cleaned in the ultraviolet ozone cleaning system for 15 minutes. All the cleaned ITO glass is next placed in the UV-Ozone cleaning instrument using ultraviolet ozone light irradiation for 15 minutes to obtain the UV-Ozone treated ITO anode. Subsequently, a thin layer of PEDOT: PSS was deposited through spin-coating at 4,000 rpm for the 30s on the pre-cleaned ITO-coated glass from a PEDOT: PSS aqueous solution and d annealed at 150 °C for 15 min in atmospheric air. Then the photovoltaic layers were spin-coated in a glovebox. The active layers, including binary blends (PM1:L8-BO and PM1:BTP-F3Cl) and ternary blends (PM1:L8-BO:BTP-F3Cl), were spin-coated from 15.4 mg/mL chloroform solution: the donor/acceptor weight ratio was 1:1.2 and then dissolved in chloroform solution with 0.35% additive of 1,8-diiodooctane (DIO) by volume, and stirred at 50 °C for 2 hours. The hot mixed solutions were spin-coated at 3500 rpm for 30 s, then an extra pre-annealing at 100 °C for 10 min was performed. The thickness optimal active layer measured by a Bruker Dektak XT stylus profilometer was about 110 nm. A PNDIT-F3N layer via a solution concentration of 1 mg mL^{-1} was deposited at the top of the active layer at a rate of 4000 rpm for 30 s. Finally, the top Argentum electrode of 100 nm thickness was thermally evaporated through a mask onto the cathode buffer layer under a vacuum of ～5×10^{-6} mbar. (Evaporated with the machine of Suzhou Fangsheng FS-300) The typical active area of the investigated devices was 5 mm^2.

The device with an active area of 10 mm^2 was certified at the optimized condition by the National Institute of Metrology (NIM) in Beijing, China. A non-refractive mask with a certified area of 5.142 mm^2 was used for the certification of the 10 mm^2 devices. The current-voltage characteristics of the solar cells were measured by a Keithley 2400 source meter unit under AM1.5G (100 mW cm^{-2}) irradiation from a solar simulator (Enlitech model SS-F5-3A). Solar simulator illumination intensity was determined at 100 mW cm^{-2} using a monocrystalline silicon reference cell with a KG5 filter. Short circuit currents under AM1.5G (100 mW cm^{-2}) conditions were estimated from the spectral response and convolution with the solar spectrum. The forward scan was

adopted to test the *J-V* curves, and the scan step is 0.02 V and the delay time is 1 ms. The scan mode is sweep. The external quantum efficiency was measured by a Solar Cell Spectral Response Measurement System QE-R3011(Enli Technology Co., Ltd.).

2. Figures and Tables

Table S1. Statistics of solvents and coating methods used for active layer systems with excellent efficiencies of near 19%.

| Active layers	Systems	PCEs	Processing solvents	Coating method	Ref.	Publications
PBQx-TF:eC9-2Cl:F-BTA3	Ternary	19.0%	Toluene	Spin-coating	4	*Adv. Mater.* **2021**, *33*, 2102420
PM6:L8-BO:BTP-H2	Ternary	19.2%	CF	Spin-coating	5	*Energy Environ. Sci.* **2022**, *15*, 2537
PTQ10:BTP-FTh:IDIC	Ternary	19.05%	CF	Spin-coating	6	*Adv. Mater.* **2022**, *34*, 2109516
PM1:L8-BO:BTP-2F2Cl	Ternary	19.17%	CF	Spin-coating	7	*Adv. Mater.* **2022**, *34*, 2110147
D18/BS3TSe-4F:Y6-O	Ternary	19.03%	CB/CF	Spin-coating	8	*Adv Mater*, **2022**, *34*, 2202089.
PTQ10:PTVT-T:m-BTP-PhC6	Ternary	19.11%	CF	Spin-coating	9	*ACS Energy Lett.* **2022**, *7*, 2547
D18/L8-BO	Binary	19.05%	CB/CF	Spin-coating	10	*Adv. Mater.* **2022**, *34*, 2204718.
PM6:D18:L8-BO	Ternary	19.6%	CF	Spin-coating	11	*Nat. Mater.* **2022**, *21*, 656
PM6:L8-BO:BTP-S10	Ternary	19.26%	CF	Spin-coating	12	*Adv. Energy Mater.* **2022**, 2201076
PM6:D18-Cl:L8-BO	Ternary	19.22%	CF	Spin-coating	13	*Adv. Sci.* **2022**, 2203606
PM6:L8-BO:BTP-eC9	Ternary	19.35%	CF	Spin-coating	14	*Adv. Mater.* **2022**, 2205844
PM1:L8-BO:BTP-F3Cl	Ternary	18.8%	THF	Blade-coating		This work
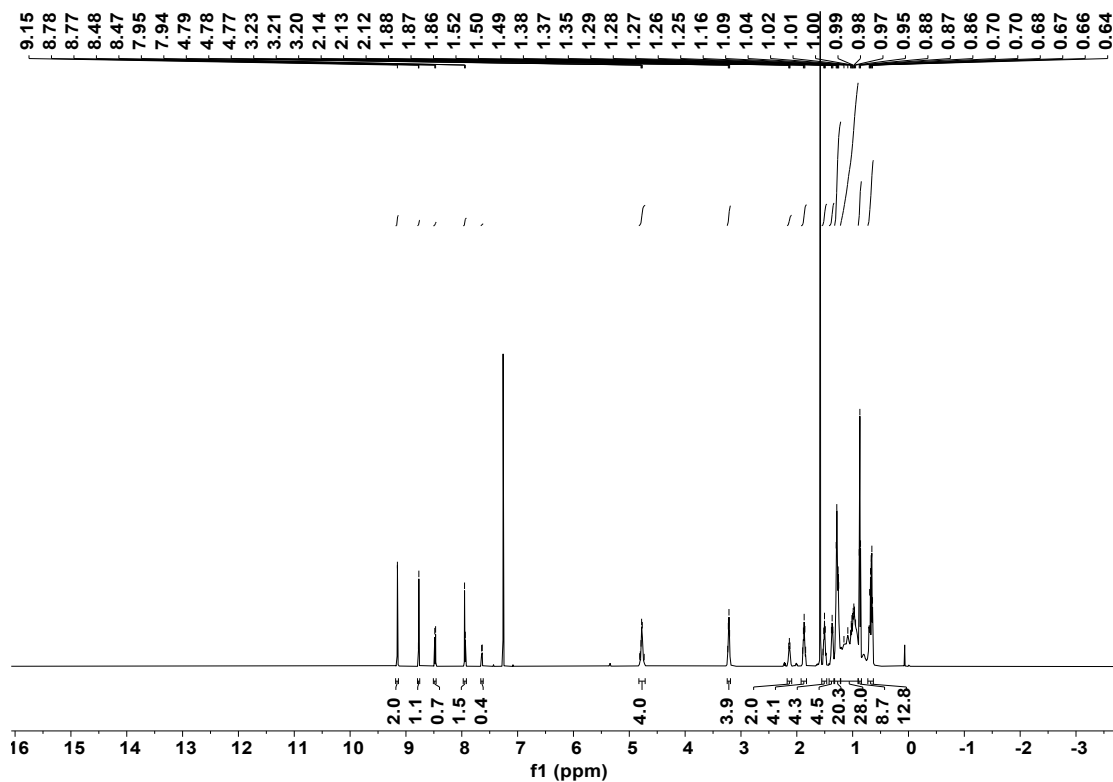
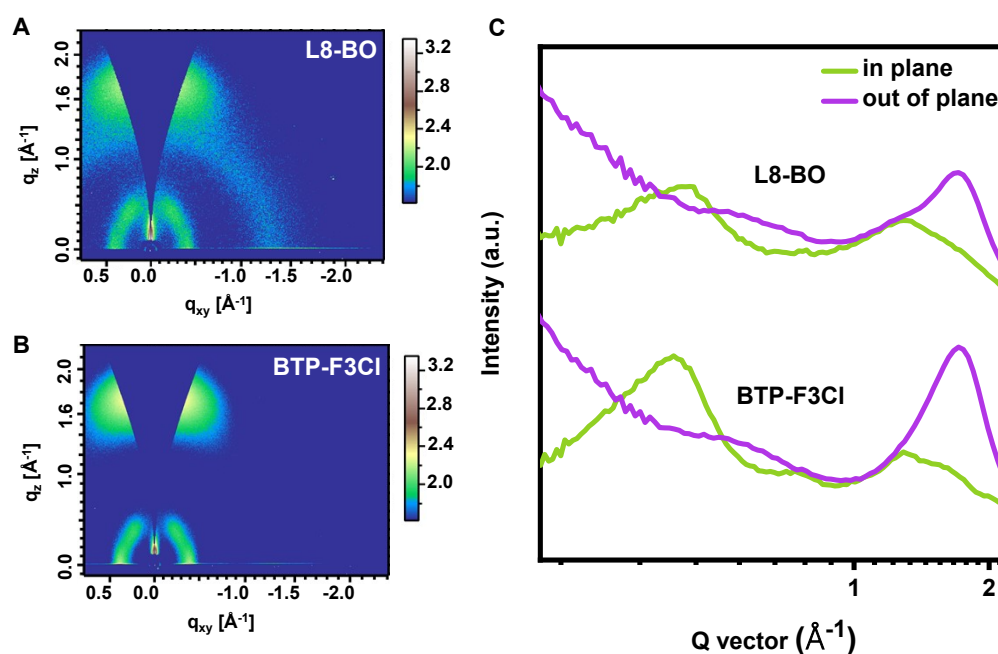**Figure S1**. ^{1}H NMR spectrum of compound BTP-F3Cl in CDCl$_3$.
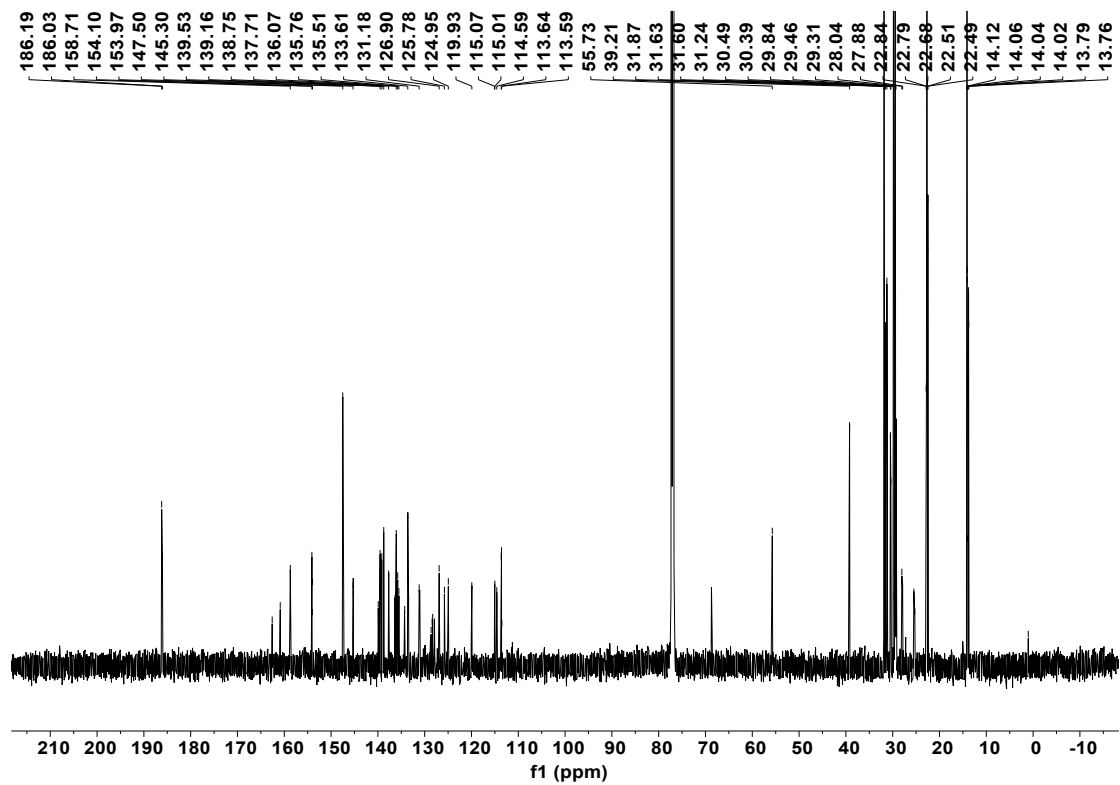
Figure S2. ^{13}C NMR spectra spectrum of compound BTP-F3Cl.
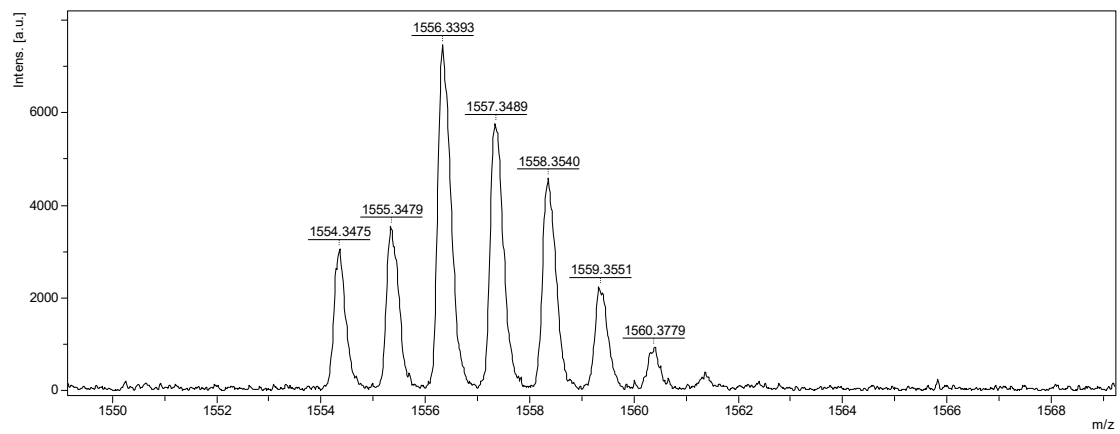
Figure S3. MALDI-TOF MS analyses of BTP-F3Cl.
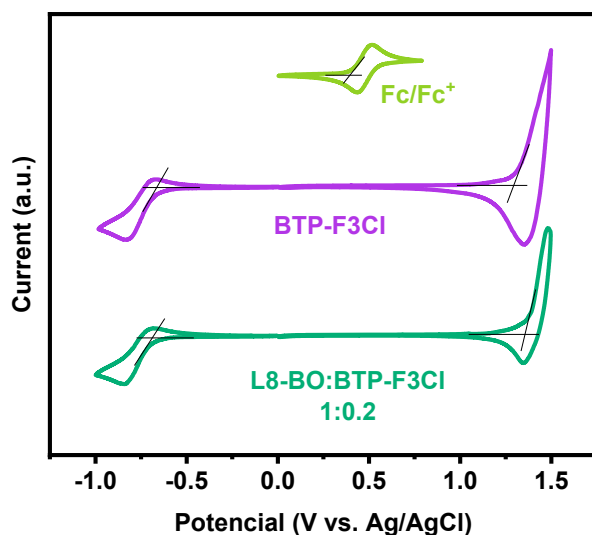
Figure S4. Cyclic voltammogram of BTP-F3Cl and L8-BO:BTP-F3Cl (1:0.2, wt%) in acetonitrile solution with 0.1 Mn-Bu$_4$PF$_6$ as the supporting electrolyte with a scanning rate of 100 mV s^{-1}.

Figure S5. 2D GIWAXS patterns of (A) pristine L8-BO and (B) BTP-F3Cl films, (C) IP and OOP extracted line-cut profiles of relevant films.

Table S2. Investigations of the morphology parameters extracted from the GIWAXS measurements of the L8-BO and BTP-F3Cl neat films.

Neat films	In plane (100)		Out of plane (010)			
	q (Å^{-1})	d (Å)	q (Å^{-1})	d (Å)	FWHM (Å^{-1})	CCL (Å)
L8-BO	0.42	14.96	1.71	3.67	0.34	16.63
BTP-F3Cl	0.39	16.11	1.72	3.65	0.29	19.50
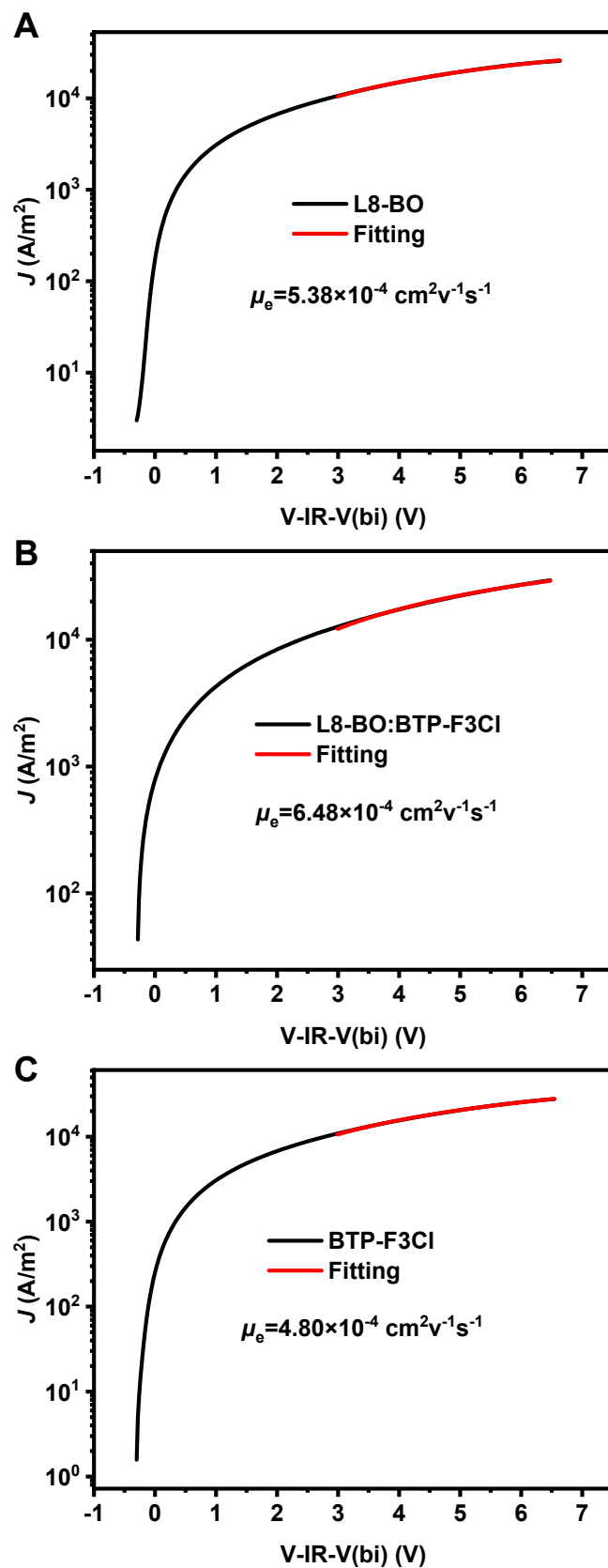
Figure S6. The dark *J-V* characteristics of (A) L8-BO, (B) L8-BO:BTP-F3Cl (1:0.2, wt%), and (C) BTP-F3Cl based electron-only devices . The red solid lines represent the best fitting using the SCLC model.
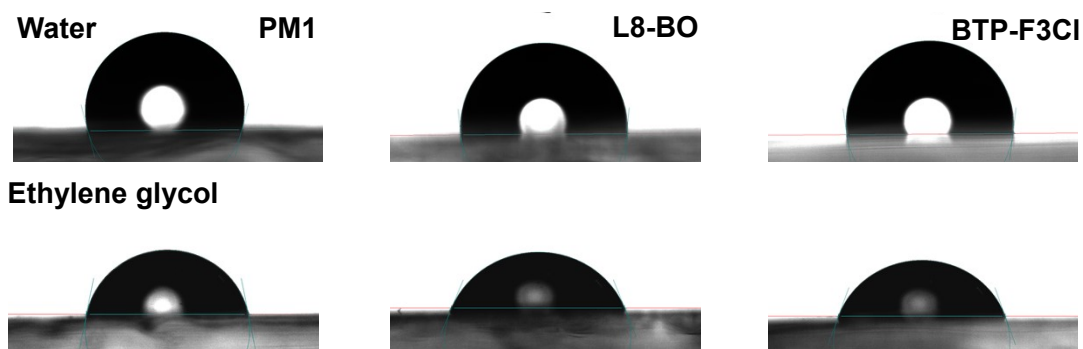
Figure S7. Photographs of water and ethylene glycol droplets on the top surfaces of the pure PM1, L8-BO and BTP-F3Cl films.

Table S3. Investigations of the contact angles, surface energy, wetting coefficient and interfacial tension values of PM1, L8-BO and BTP-F3Cl.

Materials	Contact		Surface energy [mJ m^{-2}]	Relative χ	
	Water	Ethylene glycol		(With PM1)	(With L8-BO)
PM1	104.5 (104.2±0.05)	78.6 (78.4±0.06)	35.99 (35.76±0.06)	/	/
L8-BO	95.6 (95.3±0.07)	67.2 (67.1±0.05)	41.44 (41.11±0.07)	0.19 K	/
BTP-F3Cl	97.9 (97.6±0.06)	69.0 (68.7±0.05)	43.73 (43.63±0.07)	0.38 K	0.03 K
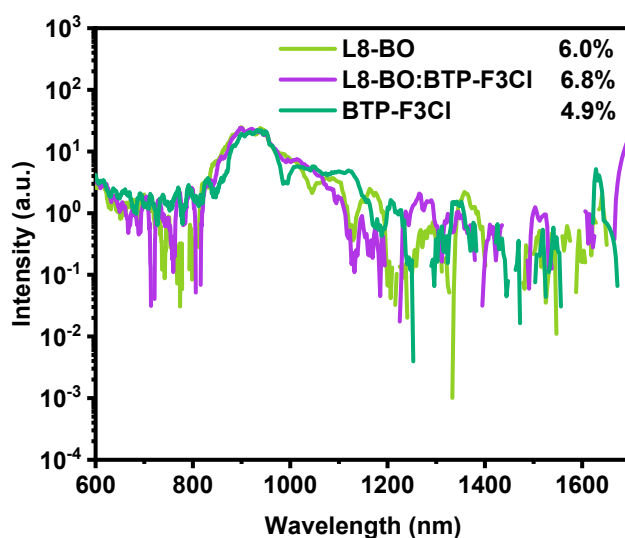
Figure S8. The photoluminescence quantum yield of the L8-BO, BTP-F3Cl and their

blend (L8-BO:BTP-F3Cl, 1:0.2, wt%).
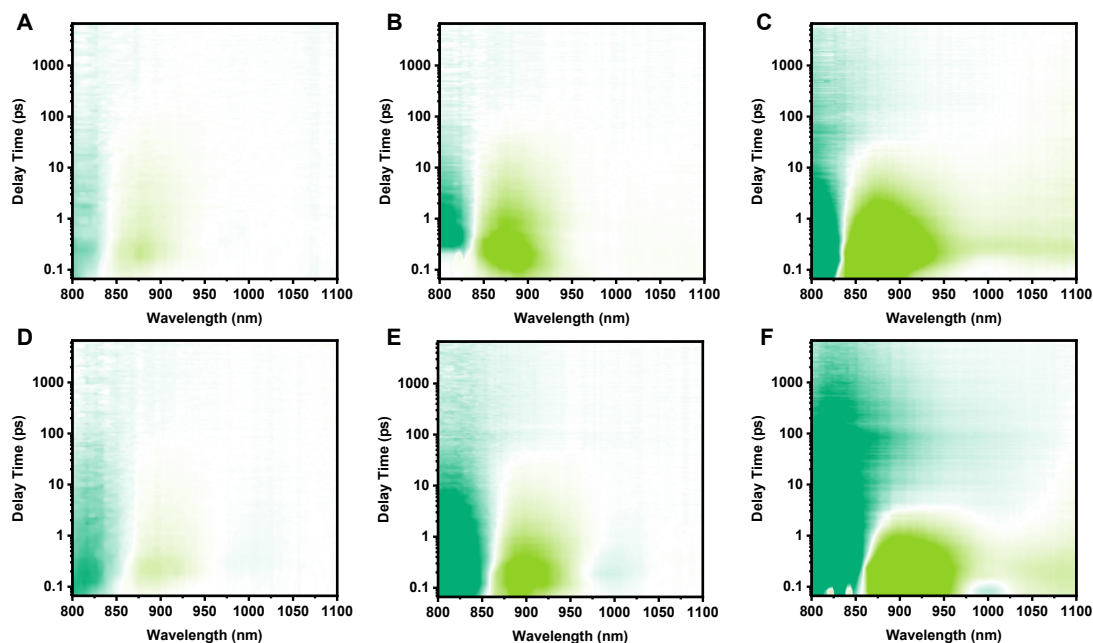
Figure S9. The TA images of (A-C) L8-BO neat film and (D-F) L8-BO:BTP-F3Cl film under 800 nm pump with power flux of 2, 8 and 24 μJ cm^{-2}.
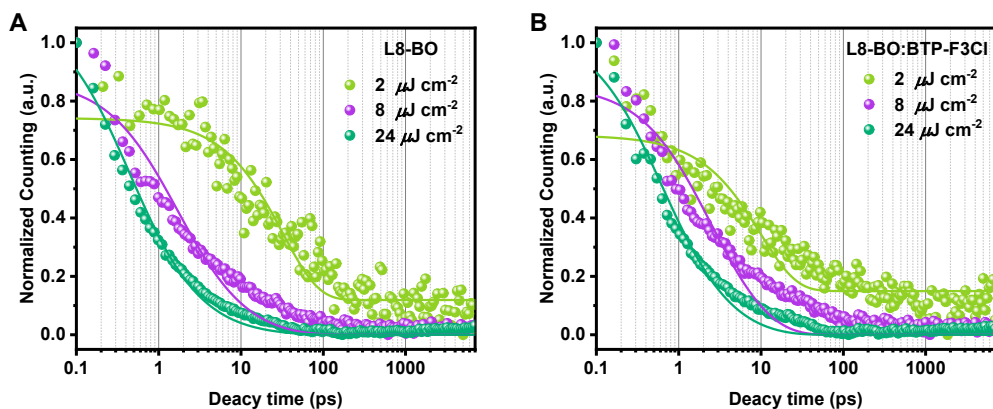
Figure S10. Exciton diffusion length measurements. The dynamics of the singlet excitons measured with the 800 nm pump excitation at different densities in films of (A) L8-BO and (B) L8-BO:BTP-F3Cl. The fluence-dependent singlet exciton decays are fitted to the exciton annihilation model (Eq. (2)).

Table S4. Detailed parameters of single exciton decay dynamic for neat and the alloy acceptor films.

Materials	k (10^{-3} ps)	α (nm^3 ps^{-1})	τ (ps)	D (nm^2 ps^{-1})	L_D (nm)
L8-BO	31.07	401.08	32.19	15.96	22.47
L8-BO:BTP-F3Cl	101.11	2908.79	9.89	115.74	33.83

Table S5. Photovoltaic parameters of the ternary organic solar cells with different BTP-F3Cl contents, measured under the illumination of AM 1.5G at 100 mW cm^{-2}.

PM1:L8-BO:BTP-F3Cl	V_{OC} [V]	J_{SC} [mA cm^{-2}]	FF [%]	PCE[a] [%]
1:1.2:0	0.893	26.3	78.4	18.4 (18.20±0.21)
1:1:0.2	0.885	27.2	79.2	19.1 (18.85±0.17)
1:0.8:0.4	0.874	27.3	78.9	18.8 (18.65±0.18)
1:0.6:0.6	0.871	27.3	78.3	18.6 (18.44±0.22)
1:0.4:0.8	0.856	27.4	77.8	18.2 (18.04±0.17)
1:0.2:1	0.850	27.6	77.3	18.1 (17.92±0.18)
1:0:1.2	0.844	27.8	76.7	18.0 (17.79±0.22)

[a]The values in parenthesis are the average PCEs obtained from 20 devices.

Appendix: Summary of the Report
Report No.: GXgf2021-13528
Client: Wuhan University
Sample: Organic Solar Cells
Type/Model: Organic Solar Cells
DUT S/N: 7-1-M1-F-2
Manufacturer: Wuhan University
Date of Test: 10/21/2021
Temperature Sensor/Control System: None
Environmental conditions: (22±1) C°, RH (22±2) %
Mask: An aperture area of 5.142 mm² (M1, Certificate No.: CDjc2020-06913)

The test has been conducted by the PV Metrology Lab of NIM (National Institute of Metrology, China). Measurement of irradiance intensity and all other measurements are traceable to the International System of Units (SI). Data in this report apply only at the time of the test for the sample. For more details, please refer to the text of the report.

Forward Scan:

Area (mm²)	I_{sc}(mA)	V_{oc}(V)	P_{max}(mW)
5.142	1.401	0.872	0.960
I_{max}(mA)	V_{max}(V)	FF (%)	η (%)
1.264	0.760	78.6	18.7

I-V Characterization Methods:
JJF 1622-2017: Calibration Specification of Solar Cells: Photoelectric Properties
Reference Solar Cell:
Type: Mono-Si
Solar Simulator:
Classification: AAA (Double-light source: Xeon and Halogen);
Total irradiance: 1000 W/m² based on I_{sc} of the above Reference Solar Cell.
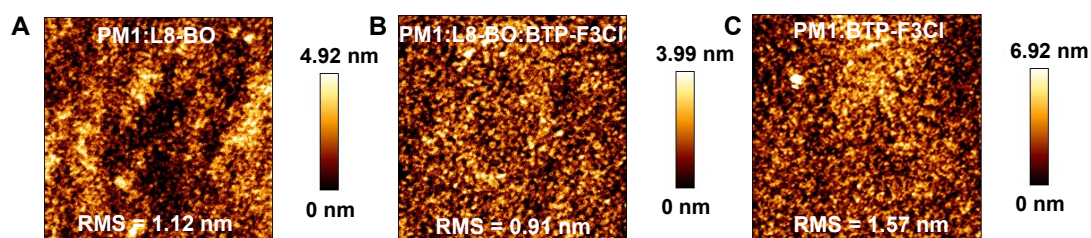
Figure S11. Report of certified efficiency of PM1:L8-BO:BTP-F3Cl solar cells from National Institute of Metrology, China.
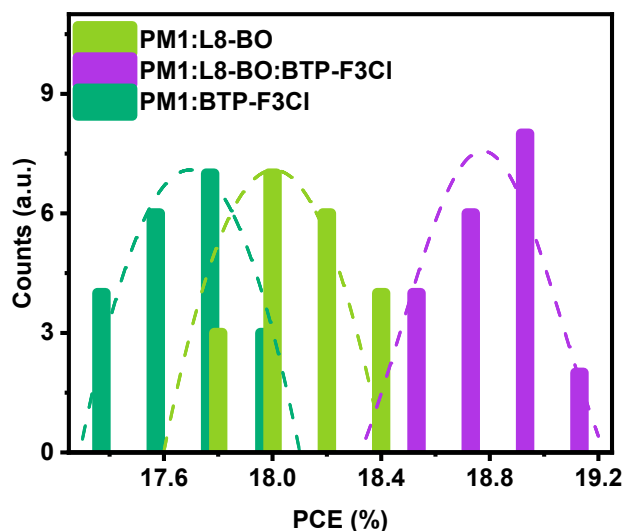
Figure S12. The efficiency distribution histogram of twenty independently devices based on PM1:L8-BO, PM1:BTP-F3Cl, and PM1:L8-BO:BTP-F3Cl, respectively.

Figure S13. AFM surface scans (5×5 um^2) of the (A) PM1:L8-BO, (B) PM1:L8-BO:BTP-F3Cl, and (C) PM1:BTP-F3Cl blends, respectively.

Table S6. Investigations of the morphology parameters extracted from the GIWAXS measurements of the binary and ternary films.

Active layers	Out-of-plane				In-plane	
	q	d-spacing	FWHM	CCL	q	d-spacing
	($Å^{-1}$)	($Å^{-1}$)	($Å^{-1}$)	($Å$)	($Å^{-1}$)	($Å^{-1}$)
PM1	1.67	3.76	0.41	13.79	0.29	21.67
PM1:L8-BO	1.72	3.65	0.31	18.24	0.30	20.93
PM1:L8-BO:BTP-F3Cl	1.71	3.67	0.29	19.50	0.30	20.93
PM1:BTP-F3Cl	1.71	3.67	0.28	20.20	0.30	20.93

Table S7. The characteristic hole transfer lifetimes of PM6:F8IC, PM6:F8IC:IT-4F and PM6:F8IC:Y6 blend films.

Active layer	τ_1 (ps)	τ_2 (ps)
PM1:L8-BO	0.57	0.69
PM1:L8-BO:BTP-F3Cl	0.46	0.56
PM1:BTP-F3Cl	0.93	1.14

**Table S8.** The parameters of exciton dissociation efficiency and charge collection efficiency.

Device	Exciton dissociation efficiency (%)	G_{max} (m^{-3}s^{-1})
PM1:L8-BO	98.0	1.69×10^{28}
PM1:L8-BO:BTP-F3Cl	98.5	1.75×10^{28}
PM1:BTP-F3Cl	97.8	1.78×10^{28}

Table S9. Parameters of electron mobility, hole mobility and carrier mobility of PM1:L8-BO and PM1:L8-BO:BTP-F3Cl and PM1:BTP-F3Cl devices.

Device	μ_e (×10^{-4} cm^2 V^{-1} s^{-1})	μ_h (×10^{-4} cm^2 V^{-1} s^{-1})	$\mu_{carrier}$ (×10^{-4} cm^2 V^{-1} s^{-1})	μ_h/μ_e
PM1:L8-BO	6.53±0.28	7.46±0.26	2.73	1.14
PM1:L8-BO:BTP-F3Cl	7.88±0.26	8.56±0.25	3.04	1.09
PM1:BTP-F3Cl	4.54±0.29	6.21±0.28	2.39	1.37
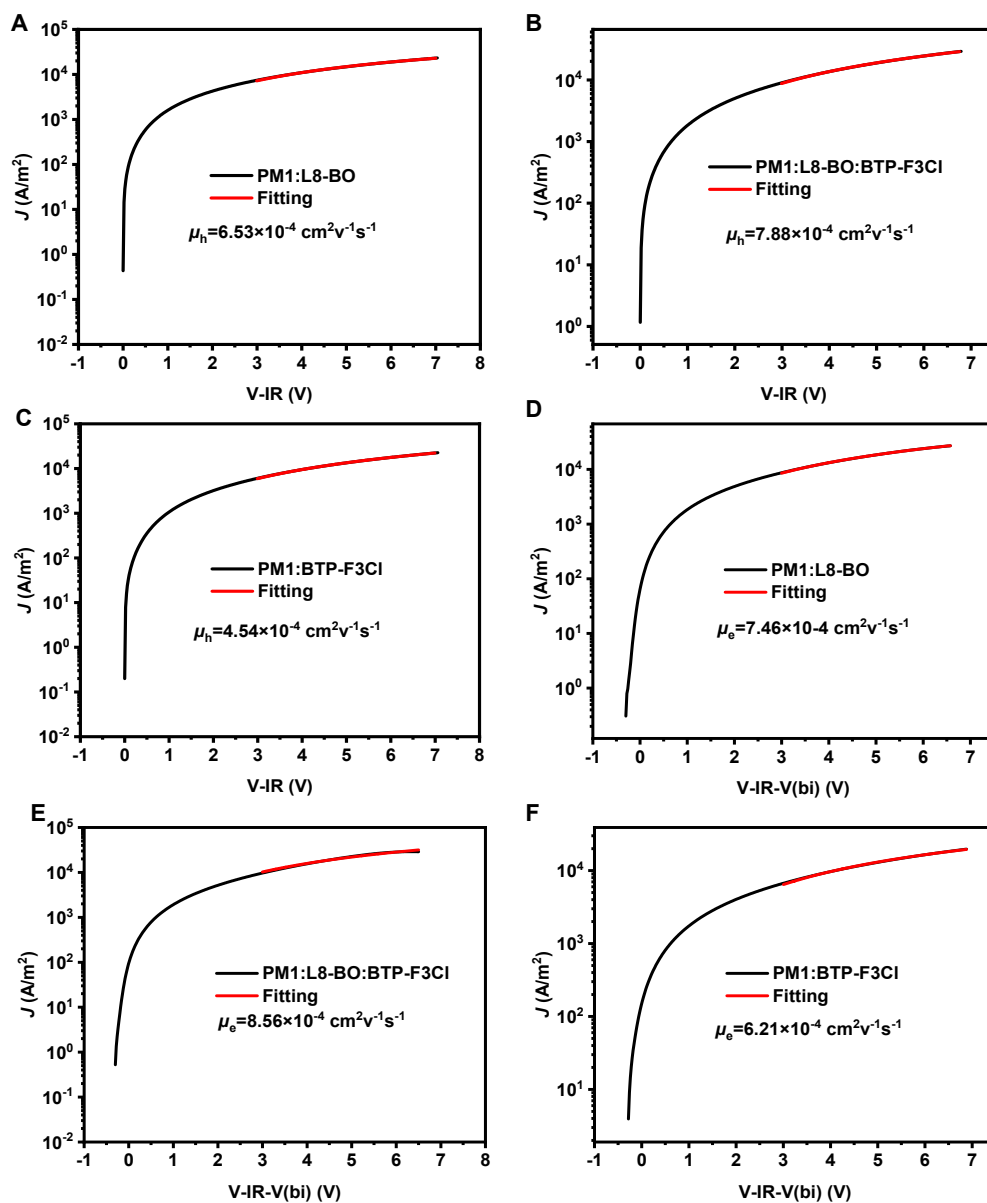
Figure S14. The dark *J-V* characteristics of PM1:L8-BO, PM1:L8-BO:BTP-F3Cl and PM1:BTP-F3Cl based hole-only devices and electron-only devices. The red solid lines represent the best fitting using the SCLC model.
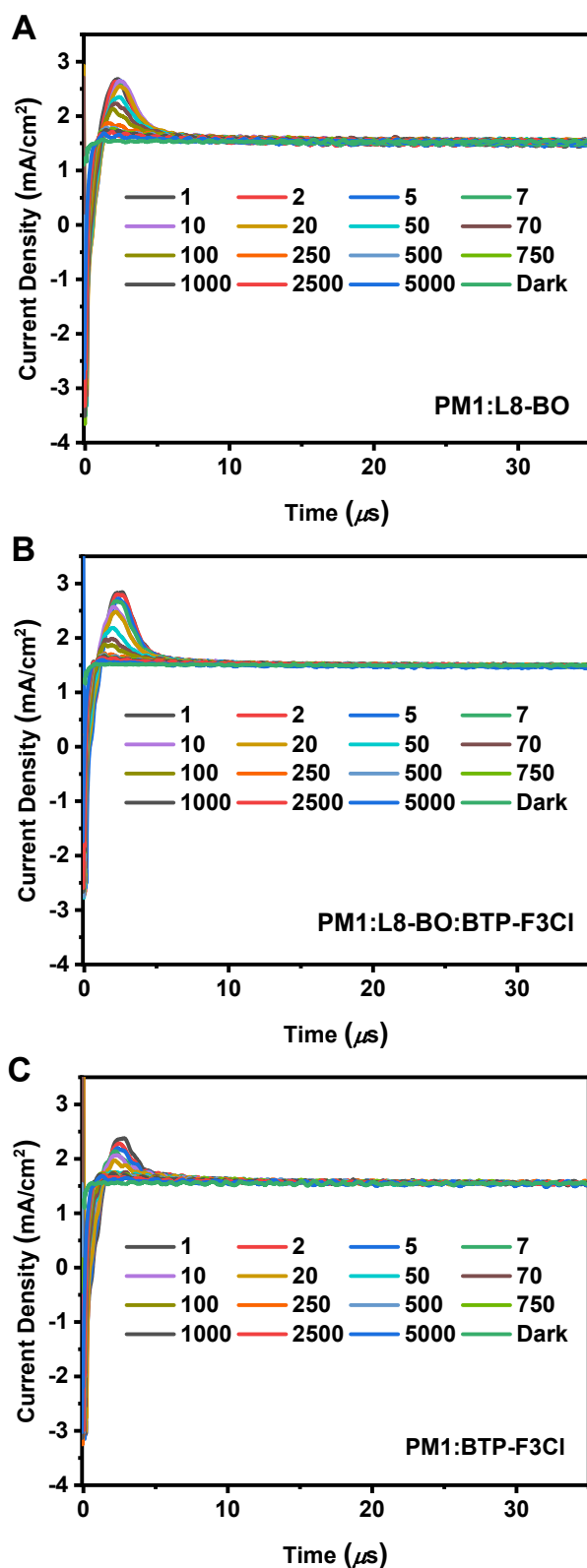
Figure S15. The photo-CELIV traces for (A) PM1:L8-BO, (B) PM1:L8-BO:BTP-F3Cl and (C) PM1:BTP-F3Cl devices for different delay times between the light pulse and the extraction voltage ramp.
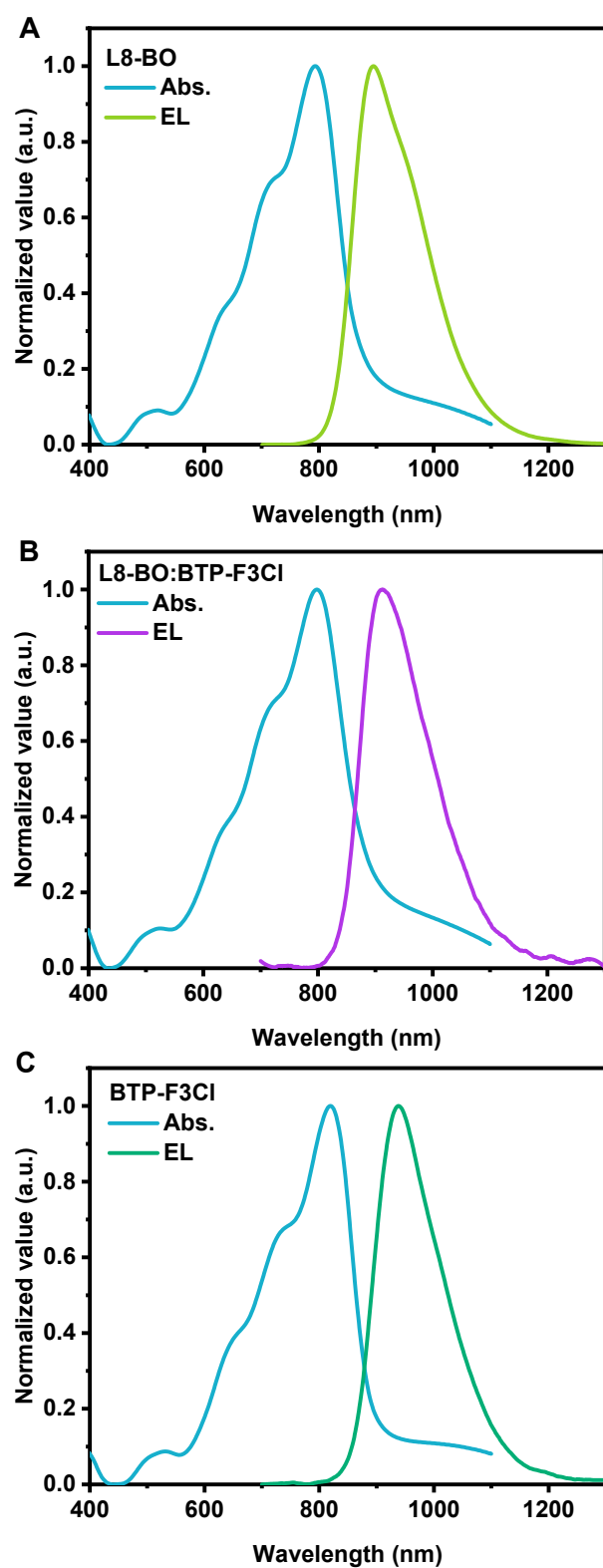
Figure S16. Emission and absorption spectra of the (A) L8-BO, (B) L8-BO:BTP-F3Cl and (C) BTP-F3Cl films.

Table S10. Measured and calculated parameters to quantify the non-radiative recombination losses of the optimized binary and ternary devices.

Device	$E_g{}^a$ (eV)	$V_{OC}{}^b$ (V)	E_{loss} (eV)	V_{SQ}^{OC} (V)	ΔE_1 (eV)	$V_{rad}^{OC}{}^c$ (V)	ΔE_2 (eV)	ΔE_3 (eV)	Exp. $\Delta E_3{}^d$ (eV)
PM1:L8-BO	1.457	0.893	0.564	1.199	0.258	1.091	0.108	0.198	0.205
PM1:L8-BO:BTP-F3Cl	1.434	0.885	0.549	1.178	0.256	1.071	0.107	0.186	0.193
PM1:BTP-F3Cl	1.411	0.844	0.567	1.156	0.255	1.051	0.105	0.207	0.215

[a]E_g was determined from the intersection of the EQE edge and the local EQE maximum. [b]V_{OC} was calculated from the measured J-V curves. [c]V_{rad} OC was calculated from FTPS and EL measurements. [d]Exp. ΔE_3 is calculated with the Equation ($\Delta E_3 = -kT\ln\left(EQE_{EL}\right)$).
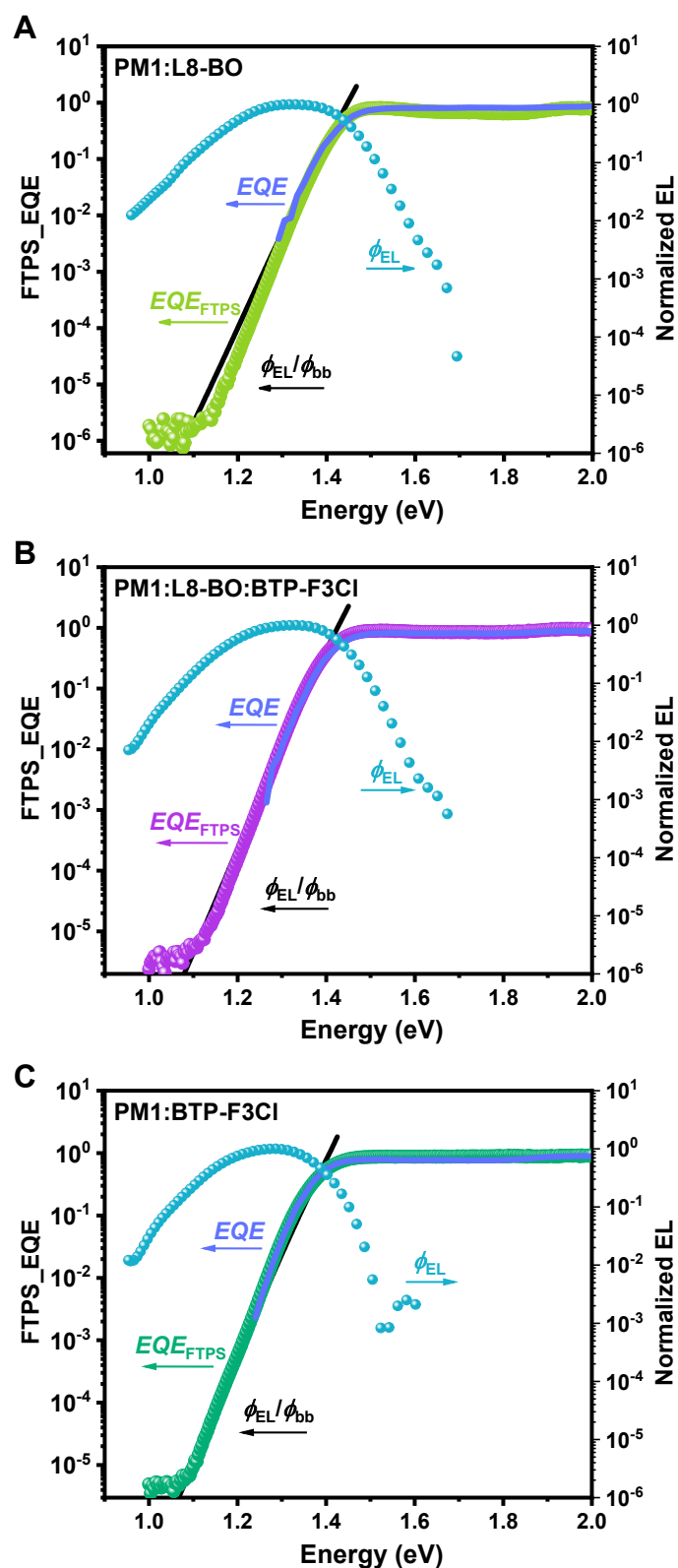
Figure S17. Semi-logarithmic plots of normalized EL, measured EQE and EQE calculated by FTPS (EQE$_{FTPS}$) as a function of energy for devices based on (A) PM1:L8-BO, (B) PM1:L8-BO:BTP-F3Cl and (C) PM1:BTP-F3Cl blends. The ratio of ϕ_{EL}/ϕ_{bb} was used to plot the EQE in the low-energy regime, where ϕ_{EL} and ϕ_{bb} represent the emitted photon flux and the room-temperature blackbody photon flux, respectively.
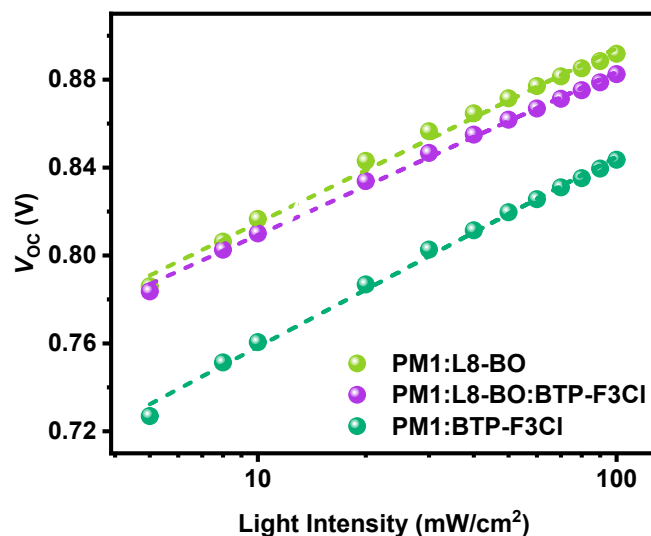
Figure S18. Curves of V_{OC} versus P_{light}. Charge recombination kinetics of the binary and ternary devices were investigated as well. Generally, when the dominant mechanism is bimolecular recombination, a slope of kT/q (where k is the Boltzmann's constant, T is the temperature in Kelvins, and q is the elemental charge) is expected. In this work, slopes of 1.34, 1.25, and 1.45 kT/q were obtained for PM1:L8-BO, PM1:L8-BO:BTP-F3Cl, and PM1:BTP-F3Cl devices, respectively. This result suggests that a small amount of BTP-F3Cl in ternary blends can effectively deactivate traps in the host blend and thereby suppress trap-assisted recombination.
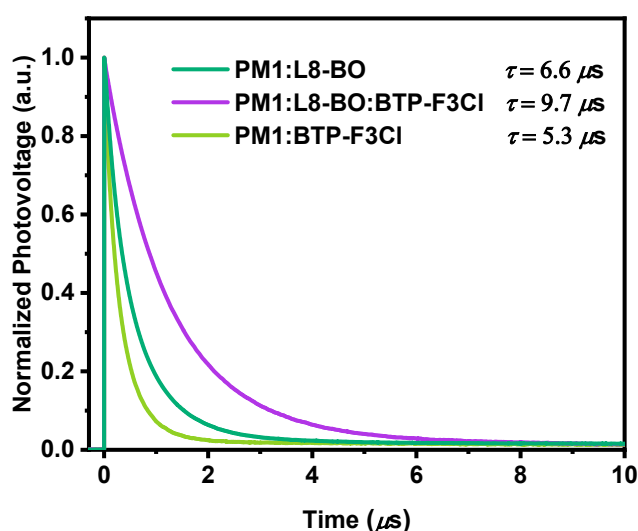
Figure S19. Transient photovoltage (TPV) curves of the binary and ternary devices. Moreover, TPV measurements were conducted to study the charge recombination dynamics of the binary and ternary devices. The calculated carrier lifetime values are 6.6 μs for PM1:L8-BO, 5.3 μs for PM1:BTP-F3Cl, and 9.7 μs for the ternary system, respectively.
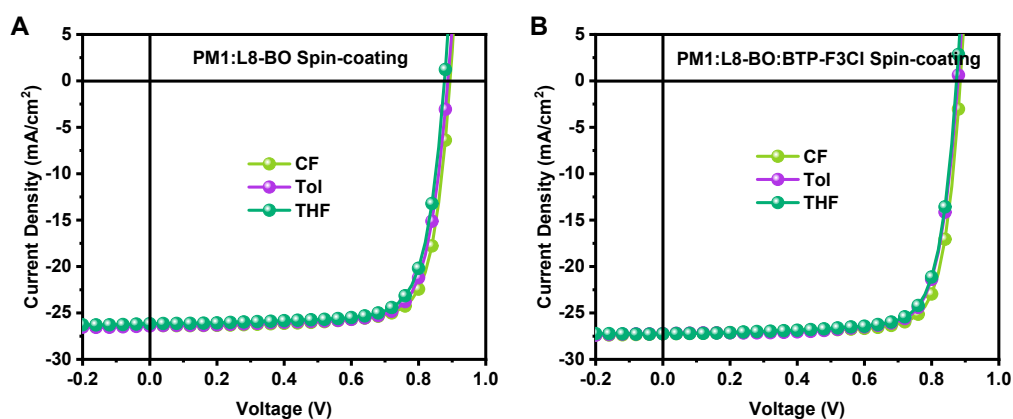
Figure S20. *J-V* characteristic curves of PM1:L8-BO and PM1:L8-BO:BTP-F3Cl processed by spin-coating with different solvents.

Table S11. Specific device performance of the binary and ternary devices under the processing condition of different solvents by spin-coating method.

Active layer	Solvents	V_{OC} [V]	J_{SC} [mA cm^{-2}]	FF [%]	PCE [%, PCE$_{avg}$[a]]
	CF	0.893	26.3	78.4	18.4 (18.20 ± 0.21)
PM1:L8-BO	Tol	0.887	26.4	77.2	18.1 (17.94 ± 0.17)
	THF	0.877	26.2	77.1	17.7 (17.55 ± 0.18)
	CF	0.885	27.2	79.2	19.1(18.85 ± 0.17)
PM1:L8-BO:BTP-F3Cl	Tol	0.879	27.2	77.8	18.6 (18.43 ± 0.18)
	THF	0.874	27.2	77.5	18.5 (18.34 ± 0.19)

[a]Average values with standard deviation are obtained from 15 devices.
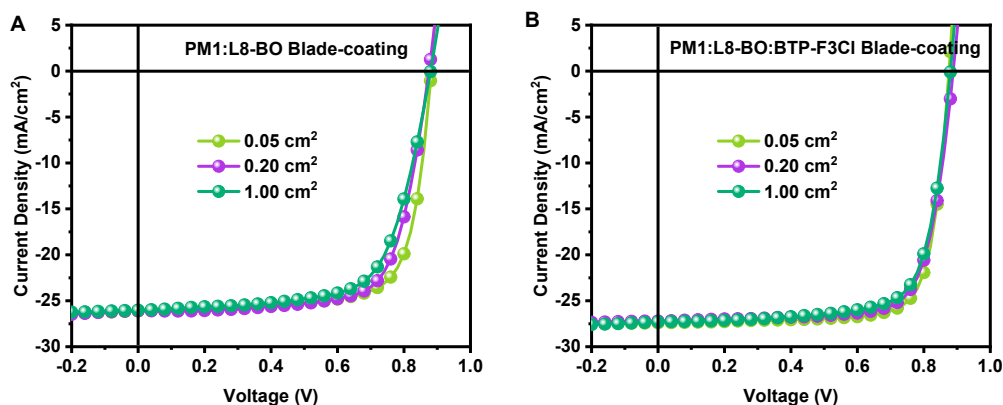
Figure S21. *J-V* characteristic of PM1:L8-BO and PM1:L8-BO:BTP-F3Cl processed by THF based on different effective areas.

Table S12. Specific device performance of PM1:L8-BO and PM1:L8-BO:BTP-F3Cl processed with THF based on different effective areas obtained by blade-coating method.

Active layer	Area	V_{OC}	J_{SC}	FF	PCE
	[cm^2]	[V]	[mA cm^{-2}]	[%]	[%, PCE$_{avg}$[a]]
	0.05	0.882	26.1	74.3	17.1 (16.92 ± 0.22)
PM1:L8-BO	0.20	0.875	26.1	71.9	16.4 (16.21 ± 0.17)
	1.00	0.880	26.0	67.8	15.5 (15.37 ± 0.18)
	0.05	0.876	27.4	78.4	18.8(18.59 ± 0.19)
PM1:L8-BO:BTP-F3Cl	0.20	0.888	27.2	75.4	18.2(18.02 ± 0.18)
	1.00	0.880	27.3	74.2	17.8 (17.63 ± 0.19)

[a]Average values with standard deviation are obtained from 15 devices.

Table S13. The summary of the PCE evolution of the doctor-blade processed OPVs in the past years.

Active layers	V_{OC} [V]	J_{SC} [mA cm^{-2}]	FF [%]	PCE [%]	References
PTB7-Th:F10IC2	0.766	23.8	68.5	12.5	15
PTB7-Th:F10IC2	0.753	22.6	67.1	11.4	15
PBDB-T-2F:IT-4F	0.86	21.3	76	13.9	16
PBDB-T:ITIC	0.90	17.4	69	10.9	16
PBDB-T:IT-M	0.94	16.9	71	11.3	16
PBDB-T:IDIC	0.98	15.5	60	9.10	16
PM6:IT-4F	0.82	18.9	64	9.9	17
PM6:IT-4F:N2200	0.86	20.8	73	12.8	17
PM6:Y6	0.81	24.4	66	12.6	17
PM6:Y6:N2200	0.83	26.3	74	15.6	17
PM6:IT-4F	0.88	20.76	72.00	13.64	18
PTB7-Th:PC$_{71}$BM	0.79	16.39	69	9.33	19
PBDB-TF:IT-4F	0.86	20.80	72	12.88	19
PM6:Y6	0.819	26.16	65.26	14.55	20
PM6:Y6	0.833	26.25	68.86	15.50	20
PBDB-T:IT-M	0.73	24.61	65.51	12.02	21
PBDB-T:ITIC	0.885	17.14	66.10	10.03	22
FTAZ:IT-M	0.940	14.4	61.9	9.1	23
FTAZ:IT-M	0.943	15.7	62.3	9.6	23
FTAZ:IT-M	0.950	16.8	66.1	11	23
PBTA-TF:ITCC	1.00	15.54	67	10.4	24
PBTA-TF:IT-M	0.97	17.76	71	12.2	24
PBTA-TF:IT-4F	0.73	20.24	72	10.6	24
PBDB-T:IT-M	0.88	14.9	72	9.42	25
PBDB-T:IT-M	0.91	15.7	72	10.3	25
PBDB-T:IT-M	0.93	16.8	76	11.8	25
PBDB-T-SF:IT-4F	0.87	20.13	70.11	12.30	26
PCE10:Y8	0.703	20.53	60.65	8.75	27
PCE10:Y8:ICBA	0.722	20.97	62.29	9.52	27

PBDTT-C-T:PC$_{71}$BM	0.68	13.96	0.40	3.78	28
PBDTT-C-T:PC$_{71}$BM	0.76	16.88	0.43	5.57	28
PBDTT-C-T:PC$_{71}$BM	0.77	16.12	0.41	5.05	28
PBDB-T:FOIC:IT-M	0.721	22.64	63.46	10.45	29
PT2:Y6	0.83	26.3	68.90	15.00	30
J71:ITC6-IC	0.950	16.15	67.79	10.41	31
PffBT4T-2OD: PC$_{71}$BM	0.77	18.4	70	9.9	32
PBDTTT-EFT: PC$_{71}$BM	0.82	19.44	63	9.75	33
PBDTTT-EFT: PC$_{71}$BM	0.85	17.39	67	9.39	33
PBDTTT-EFT: PC$_{71}$BM	0.82	17.89	74	11.09	33
PBDB-T:FOIC:IT-M	0.751	24.66	63.57	11.01	29
PM6:Y6	0.840	25.22	72.49	15.37	34
PM6:Y6-2Cl	0.847	25.67	70.74	15.38	34
PTQ10:Y6	0.855	22.62	70.32	13.62	34
PM6:Y6-C2	0.844	25.76	71.69	15.59	34
J71/ITC6-IC	0.968	16.85	70.10	11.47	31
J71/ITC6-IC	0.960	17.61	67.54	11.42	35
PTQ10/IDIC	0.952	17.14	69.13	11.28	35
PM6/Y6	0.834	25.90	75.68	16.35	34
PM6/Y6-2Cl	0.849	25.88	72.30	15.89	34
PTQ10/Y6	0.849	24.49	72.63	15.10	34
PM6/Y6-C2	0.834	25.82	73.99	15.93	34
PBDB-T:PTB7-Th:FOIC	0.73	24.61	65.51	12.02	36
PBDB-T:PYSe-TC6T(10)	0.889	22.48	64.21	12.83	37
PBDB-TF:IT-4F	0.849	21.09	75.67	13.55	38
PBDB-T:m-ITIC-O-EH	0.86	16.61	68	9.68	39
P2F-EHp:IT-4F:IT-4Cl	0.86	17.78	65.77	10.1	40
PBDB-T:IT-M/PBDB-T:FOIC	0.751	24.66	63.57	11.91	41
PBDB-TF:BTP-4Cl-16	0.833	26.0	71.6	15.5	42
PBDB-TF:BTP-eC9	0.832	25.7	75.9	16.2	43
PM6:BTP-eC9	0.83	24.9	73	15.1	44
PBDT-DTBTO/INPIC-4F	0.797	23.3	67.7	12.6	45

PM6:Y6	0.834	24.95	74.55	15.51	46
PTQ10:Y6	0.823	26.52	73.38	16.02	47
PM6:Y6	0.839	26.22	73.52	16.17	48
PM6/BTP-eC9	0.836	26.26	76.4	16.77	49
PBDB-T:PTClo-Y	0.946	19.99	65.7	12.42	50
PM6:BTP-eC9	0.84	26.77	76.33	17.15	51
PM6:BTP-eC9	0.799	26.25	73.6	15.5	52
PYSe-TCl20:PTClo-Y	0.908	22.3	68.1	13.81	53
PM6:Y6:PC$_{70}$BM	0.84	20.97	64	11.32	54
PBDB-TF:BTP-eC9	0.831	26.7	75.5	16.9	55
PM6:BTP-BO-4Cl	0.85	27.23	73.96	17.12	56
PM6:IT-M/BTP-eC9	0.855	26.34	76.20	17.16	57
PM6/Y6	0.837	25.89	75.00	16.26	58
PM6:BTP-eC9	0.840	26.37	74.81	16.58	59

References.

1   S. Chandrabose, K. Chen, A. J. Barker, J. J. Sutton, S. K. K. Prasad, J. Zhu, J. Zhou, K. C. Gordon, Z. Xie, X. Zhan and J. M. Hodgkiss, *J. Am. Chem. Soc.,* 2019, **141**, 6922.

2   P. Bi, S. Zhang, Z. Chen, Y. Xu, Y. Cui, T. Zhang, J. Ren, J. Qin, L. Hong, X. Hao and J. Hou, *Joule*, 2021, **5**, 2408.

3   O. Mikhnenko, P. Blom, T.-Q. T. Nguyen, *Energy Environ. Sci.,* 2015, **8**, 1867.

4   Y. Cui, Y. Xu, H. Yao, P. Bi, L. Hong, J. Zhang, Y. Zu, T. Zhang, J. Qin, J. Ren, Z. Chen, C. He, X. Hao, Z. Wei and J. Hou, *Adv. Mater.,* 2021, **33**, 2102420.

5   C. He, Y. Pan, Y. Ouyang, Q. Shen, Y. Gao, K. Yan, J. Fang, Y. Chen, C.-Q. Ma, J. Min, C. Zhang, L. Zuo and H. Chen, *Energy Environ. Sci.,* 2022, **15**, 2537.

6   K. Chong, X. Xu, H. Meng, J. Xue, L. Yu, W. Ma and Q. Peng, *Adv. Mater.,* 2022, **34**, 2109516.

7   R. Sun, Y. Wu, X. Yang, Y. Gao, Z. Chen, K. Li, J. Qiao, T. Wang, J. Guo, C. Liu, X. Hao, H. Zhu and J. Min, *Adv. Mater.,* 2022, **34**, 2110147.

8   W. Gao, F. Qi, Z. Peng, F. R. Lin, K. Jiang, C. Zhong, W. Kaminsky, Z. Guan, C. S. Lee, T. J. Marks, H. Ade and A. K. Jen, *Adv. Mater.,* 2022, **34**, 2202089.

9   R. Ma, C. Yan, J. Yu, T. Liu, H. Liu, Y. Li, J. Chen, Z. Luo, B. Tang, X. Lu, G. Li and H. Yan, *ACS Energy Lett.,* 2022, **7**, 2547.

10 Y. Wei, Z. Chen, G. Lu, N. Yu, C. Li, J. Gao, X. Gu, X. Hao, G. Lu, Z. Tang, J. Zhang, Z. Wei, X. Zhang and H. Huang, *Adv. Mater.,* 2022, **34**, 2204718.

11 L. Zhu, M. Zhang, J. Xu, C. Li, J. Yan, G. Zhou, W. Zhong, T. Hao, J. Song, X. Xue, Z. Zhou, R. Zeng, H. Zhu, C. C. Chen, R. C. I. MacKenzie, Y. Zou, J. Nelson, Y. Zhang, Y. Sun and F. Liu, *Nat. Mater.,* 2022, **21**, 656.

12 L. Zhan, S. Li, Y. Li, R. Sun, J. Min, Y. Chen, J. Fang, C. Q. Ma, G. Zhou, H. Zhu, L. Zuo, H. Qiu, S. Yin and H. Chen, *Adv. Energy Mater.,* 2022, DOI: 10.1002/aenm.202201076.

13 J. Gao, N. Yu, Z. Chen, Y. Wei, C. Li, T. Liu, X. Gu, J. Zhang, Z. Wei, Z. Tang, X. Hao, F. Zhang, X. Zhang and H. Huang, *Adv. Sci.*, 2022, DOI:

10.1002/advs.202203606.

14 S. Guan, Y. Li, K. Yan, W. Fu, L. Zuo and H. Chen, *Adv. Mater.,* 2022, DOI: 10.1002/adma.202205844.

15 X. Han, J. Zhu, Y. Xiao, H. Jiang, Z. Zhang, J. Wang, Z. Li, Y. Lin, X. Lu and X. Zhan, *Solar RRL,* 2020, **4**, 2000108.

16 Q. Kang, L. Ye, B. Xu, C. An, S. J. Stuard, S. Zhang, H. Yao, H. Ade and J. Hou, *Joule,* 2019, **3**, 227.

17 S. Dong, K. Zhang, T. Jia, W. Zhong, X. Wang, F. Huang and Y. Cao, *EcoMat*, **2019**, *1*, 12006.

18 L. Zhang, H. Zhao, B. Lin, J. Yuan, X. Xu, J. Wu, K. Zhou, X. Guo, M. Zhang and W. Ma, *J. Mater. Chem. A,* 2019, **7**, 22265.

19 G. Ji, W. Zhao, J. Wei, L. Yan, Y. Han, Q. Luo, S. Yang, J. Hou and C.-Q. Ma, *J. Mater. Chem. A,* 2019, **7**, 212.

20 J. Yuan, D. Liu, H. Zhao, B. Lin, X. Zhou, H. B. Naveed, C. Zhao, K. Zhou, Z. Tang, F. Chen and W. Ma, *Adv. Energy Mater.,* 2021, **11**, 2100098.

21 L. Zhang, X. Xu, B. Lin, H. Zhao, T. Li, J. Xin, Z. Bi, G. Qiu, S. Guo, K. Zhou, X. Zhan and W. Ma, *Adv. Mater.,* 2018, **30**, 1805041.

22 L. Zhang, B. Lin, B. Hu, X. Xu and W. Ma, *Adv. Mater.,* 2018, **30**, 1800343.

23 L. Ye, Y. Xiong, Q. Zhang, S. Li, C. Wang, Z. Jiang, J. Hou, W. You and H. Ade, *Adv. Mater.,* 2018, **30**, 1705485.

24 W. Zhao, S. Zhang, Y. Zhang, S. Li, X. Liu, C. He, Z. Zheng and J. Hou, *Adv. Mater.,* 2018, **30**, 1704837.

25 Q. Kang, Q. Liao, Y. Xu, L. Xu, Y. Zu, S. Li, B. Xu and J. Hou, *ACS Appl. Mater. Interfaces,* 2019, **11**, 20205.

26 Q. Wu, J. Guo, R. Sun, J. Guo, S. Jia, Y. Li, J. Wang and J. Min, *Nano Energy,* 2019, **61**, 559.

27 C. Zhu, H. Huang, Z. Jia, F. Cai, J. Li, J. Yuan, L. Meng, H. Peng, Z. Zhang, Y. Zou and Y. Li, *Solar Energy,* 2020, **204**, 660.

28 Y.-H. Lee, P.-T. Tsai, C.-J. Chang, H.-F. Meng, S.-F. Horng, H.-W. Zan, H.-C. Lin, H.-C. Liu, M.-R. Tseng and H.-C. Yeh, *AIP Advances,* 2016, **6**, 115006.

29 Y. Wang, X. Wang, B. Lin, Z. Bi, X. Zhou, H. B. Naveed, K. Zhou, H. Yan, Z. Tang and W. Ma, *Adv. Energy Mater.,* 2020, **10**, 200826.

30 K. Weng, L. Ye, L. Zhu, J. Xu, J. Zhou, X. Feng, G. Lu, S. Tan, F. Liu and Y. Sun, *Nat. Commun.,* 2020, **11**, 2855.

31 R. Sun, J. Guo, Q. Wu, Z. Zhang, W. Yang, J. Guo, M. Shi, Y. Zhang, S. Kahmann, L. Ye, X. Jiao, M. A. Loi, Q. Shen, H. Ade, W. Tang, C. J. Brabec and J. Min, *Energy Environ. Sci.,* 2019, **12**, 3118.

32 H. W. Ro, J. M. Downing, S. Engmann, A. A. Herzing, D. M. DeLongchamp, L. J. Richter, S. Mukherjee, H. Ade, M. Abdelsamie, L. K. Jagadamma, A. Amassian, Y. Liu and H. Yan, *Energy Environ. Sci.,* 2016, **9**, 2835.

33 S.-H. Chen, C. H. Liao, C. Y. Chang, K. M. Huang, J. Y. Chen, C. H. Chen, H.-F. Meng, H.-W. Zan, S.-F. Horng, Y.-C. Lin and M.-H. Yeh, *Org. Electron.,* 2019, **75**, 105376.

34 R. Sun, Q. Wu, J. Guo, T. Wang, Y. Wu, B. Qiu, Z. Luo, W. Yang, Z. Hu, J. Guo, M. Shi, C. Yang, F. Huang, Y. Li and J. Min, *Joule,* 2020, **4**, 407.

35 R. Sun, J. Guo, C. Sun, T. Wang, Z. Luo, Z. Zhang, X. Jiao, W. Tang, C. Yang, Y. Li and J. Min, *Energy Environ. Sci.,* 2019, **12**, 384.

36 L. Zhang, X. Xu, B. Lin, H. Zhao, T. Li, J. Xin, Z. Bi, G. Qiu, S. Guo, K. Zhou, X. Zhan and W. Ma, *Adv. Mater.,* 2018, **30**, 1805041.

37 J. Liu, J. Liu, J. Deng, B. Huang, J. Oh, L. Zhao, L. Liu, C. Yang, D. Chen, F. Wu and L. Chen, *J. Energy Chem.,* 2022, **71**, 631.

38 W. Zhao, Y. Zhang, S. Zhang, S. Li, C. He and J. Hou, *J. Mater. Chem. C,* 2019, **7**, 3206.

39 S. Lee, K. H. Park, J. H. Lee, H. Back, M. J. Sung, J. Lee, J. Kim, H. Kim, Y. H. Kim, S. K. Kwon and K. Lee, *Adv. Energy Mater.,* 2019, **9**, 1900044.

40 K. An, W. Zhong, L. Ying, P. Zhu, B. Fan, Z. Li, N. Li, F. Huang and Y. Cao, *J. Mater. Chem. C,* 2020, **8**, 270.

41 Y. Wang, X. Wang, B. Lin, Z. Bi, X. Zhou, H. B. Naveed, K. Zhou, H. Yan, Z. Tang and W. Ma, *Adv. Energy Mater.,* 2020, **10**, 2000826.

42 Y. Cui, H. Yao, L. Hong, T. Zhang, Y. Tang, B. Lin, K. Xian, B. Gao, C. An, P. Bi, W. Ma and J. Hou, *Natl. Sci. Rev.,* 2020, **7**, 1239.

43 Y. Cui, H. Yao, J. Zhang, K. Xian, T. Zhang, L. Hong, Y. Wang, Y. Xu, K. Ma, C. An, C. He, Z. Wei, F. Gao and J. Hou, *Adv. Mater.,* 2020, **32**, 1908205.

44 Q. Kang, Z. Zheng, Y. Zu, Q. Liao, P. Bi, S. Zhang, Y. Yang, B. Xu and J. Hou, *Joule,* 2021, **5**, 646.

45 J. Yu, X. Liu, H. Wang, P.-C. Lin, C.-C. Chueh, R. Zhu and W. Tang, *Chem. Eng. J.,* 2021, **405**, 127033.

46 Y. Li, H. Liu, J. Wu, H. Tang, H. Wang, Q. Yang, Y. Fu and Z. Xie, *ACS Appl. Mater. Interfaces*, 2021, **13**, 10239.

47 Y. Li, L. Deng, G. Du, Y. Li, X. Zhao and W. Deng, *Org. Electron.,* 2021, **97**, 106274.

48 Y. Zheng, R. Sun, M. Zhang, Z. Chen, Z. Peng, Q. Wu, X. Yuan, Y. Yu, T. Wang, Y. Wu, X. Hao, G. Lu, H. Ade and J. Min, *Adv. Energy Mater.,* 2021, **11**, 2102135.

49 Y. Zhang, K. Liu, J. Huang, X. Xia, J. Cao, G. Zhao, P. W. K. Fong, Y. Zhu, F. Yan, Y. Yang, X. Lu and G. Li, *Nat. Commun.,* 2021, **12**, 4815.

50 D. Chen, S. Liu, X. Hu, F. Wu, J. Liu, K. Zhou, L. Ye, L. Chen and Y. Chen, *Sci. China Chem.,* 2021, **65**, 182.

51 H. Li, S. Liu, X. Wu, Q. Qi, H. Zhang, X. Meng, X. Hu, L. Ye and Y. Chen, *Energy Environ. Sci.,* 2022, **15**, 2130.

52 H. Tang, J. Lv, K. Liu, Z. Ren, H. T. Chandran, J. Huang, Y. Zhang, H. Xia, J. I. Khan, D. Hu, C. Yan, J. Oh, S. Chen, S. Chu, P. W. K. Fong, H. Chen, Z. Xiao, C. Yang, Z. Kan, F. Laquai, S. Lu and G. Li, *Mater. Today,* 2022, **55**, 46.

53 D. Chen, S. Liu, B. Huang, J. Oh, F. Wu, J. Liu, C. Yang, L. Chen and Y. Chen, *Small,* 2022, **18**, 2200734.

54 H. C. Kwon, W. Jeong, Y. S. Lee, J. H. Jang, H. S. Jeong, S. Kim, D. Song, A. Park, E. Noh, K. Lee and H. Kang, *Adv. Energy Mater.,* 2022, **12**, 2200023.

55 Y. Yang, J. Wang, P. Bi, Q. Kang, Z. Zheng, B. Xu and J. Hou, *Chem. Mater.,* 2022, **34**, 6312.

56 J. Y. Fan, Z. X. Liu, J. Rao, K. Yan, Z. Chen, Y. Ran, B. Yan, J. Yao, G. Lu, H. Zhu, C. Z. Li and H. Chen, *Adv. Mater.,* 2022, **34**, 2110569.

57 Y. Li, J. Wu, H. Tang, X. Yi, Z. Liu, Q. Yang, Y. Fu, J. Liu and Z. Xie, *ACS Appl. Mater. Interfaces,* 2022, **14**, 31054.

58 B. Zhang, F. Yang, S. Chen, H. Chen, G. Zeng, Y. Shen, Y. Li and Y. Li, *Adv. Funct. Mater.,* 2022, **32**, 2202011.

59 J. Zhang, L. Zhang, X. Wang, Z. Xie, L. Hu, H. Mao, G. Xu, L. Tan and Y. Chen, *Adv. Energy Mater.,* 2022, **12**, 2200165.